ISSN 0915-633X

NATIONAL INSTITUTE FOR FUSION SCIENCE

Negative Ion Extraction Characteristics of a Large Negative Ion Source with Double-Magnetic Filter Configuration

Y. Takeiri, A. Ando, O. Kaneko, Y. Oka, and T. Kuroda

(Received – Apr. 14, 1992)

NIFS-151 May 1992

RESEARCH REPORT
NIFS Series

NAGOYA, JAPAN

Negative ion extraction characteristics of a large negative ion source with double-magnetic filter configuration

Y. Takeiri, A. Ando, O. Kaneko, Y. Oka, and T. Kuroda

National Institute for Fusion Science, Nagoya 464-01, Japan

ABSTRACT

A multi-ampere hydrogen negative ion source with a large extraction area of 25 cm × 25 cm has been developed. This negative ion source is a volume-production-type bucket ion source which is operated with double-magnetic filter configuration. In this configuration, the fast electrons, which produce the vibrationally excited molecules, are trapped near the chamber wall by the cusp field, which is the first magnetic filter. In the central region of the arc chamber, there exist only the thermal electrons with low temperature. As a result, the negative ions are produced in the central region by dissociative attachment. A rod magnetic filter in front of the plasma grid, which is the second magnetic filter, is utilized for reducing the population of the electrons in the vicinity of the plasma grid, which are extracted together with the negative ions. By this structure the extracted electron current can be controlled independently of the H^- ion current. So far, a 1.4A of H^- ion current has been obtained with the energy of 34 keV. Negative ion extraction characteristics of this ion source, such as the arc power dependence and the gas pressure dependence, are presented.

KEYWORDS : negative ion source, negative-ion-based NBI, volume production, magnetic filter, double-magnetic filter configuration

I. INTRODUCTION

Intense negative ion sources are required for the negative-ion-based neutral beam injection (NBI) system in the next step fusion experimental devices such as ITER, NET and FER, where the injection energies are more than 500 keV. In the Large Helical Device (LHD) project[1,2], conducted by National Institute for Fusion Science, the negative-ion-based NBI system (injection power; 20MW, injection energy; 125keV for hydrogen and 250keV for deuterium) has also been proposed[3),4)].

Recent development of the negative ion source has been concentrated on the volume production type with the bucket plasma source. There are two ways of the intense negative ion source development; one is to obtain a large current from multi-holes in a large extraction area, and the other is to achieve a high-current density from a single hole. In the former, a several amperes of H^- ion current has been extracted[5)]. In the latter, the current density of 57 mA/cm^2 has been obtained from the single hole of 1.5 mm in diameter in a large bucket source[6)], and in a small bucket source 250 mA/cm^2 has been extracted from the single hole of 1 mm in diameter[7)]. It has been also reported that the H^- ion current is enhanced by injecting cesium vapor[8)], that is considered to be ascribed to the surface effect on the plasma grid. A 10 A of H^- ion current was obtained by a small amount of cesium supply to a multi-hole bucket source[9)].

In the volume-production-type negative ion source, the arc plasma is divided into two regions; one is the driver region where the vibrationally excited molecules are produced by the fast electrons with the energy of more than 40 eV, and the other is the production and extraction region where the negative ions are produced by the dissociative attachment of the thermal electrons with the energy of around 1 eV to the vibrationally excited molecules.

These two regions are usually separated by the magnetic filter field in front of the plasma grid. The magnetic filter field is generated by the permanent magnets placed inside the arc plasma (a rod filter) or outside the arc chamber (an external filter), or by the electromagnetic circuit (an electromagnetic filter). Both the electron temperature and the electron density in the production and extraction region are reduced by this filter field, and thus the negative ion yield and the extracted electron current are simultaneously affected by the filter field strength.

In these experiments, we have utilized the cusp fields of the bucket source for the magnetic filter field, and generated the another magnetic field in front of the plasma grid by the rod filter. This magnetic field, which is called the electron filter field hereinafter, separates the extraction region from the production region, and reduces only the electron density in the extraction region. As a result, the negative ion current and the extracted electron current are expected to be controlled independently. In this configuration two kinds of the magnetic filters are utilized, and thus, we call it the double-magnetic filter configuration. With this operating concept, we have developed a large bucket negative ion source with an extraction area of 25 cm × 25 cm[10].

In this paper we report the negative ion extraction characteristics of the large bucket negative ion source utilizing the double-magnetic filter configuration, such as the dependencies on an arc power, an arc voltage, a gas pressure and an extraction voltage. The arc plasma characteristics of this negative ion source are presented in detail in ref. 11.

II. STRUCTURE OF NEGATIVE ION SOURCE

A schematic diagram of the negative ion source is illustrated in Fig. 1

(a). This ion source is a volume-production-type bucket negative ion source. Magnetic cusp lines in the arc chamber are generated by permanent magnet arrays arranged as 35 mm-separation. The electron filter field, which reduces the electron density in the extraction region, is generated in front of the plasma grid by eleven internal magnetic filter rods and two external magnetic filter bars. The internal filter rods of 10 mm in diameter are water-cooled and removable. The strength of the electron filter field can be changed by selecting the number of the rods. The distance between the plasma grid and the filter rods is also adjustable. The arc chamber is divided into three sub-chambers; two chambers of 14 cm in depth and one chamber of 7 cm in depth. Thus, the depth of the arc chamber can be changed from 19 to 40 cm by combination of these sub-chambers. The cross section of the arc chamber is 35×35 cm^2. The arc sub-chambers are made of copper with water cooling. Forty feedthroughs for filaments are attached to one of the 14 cm-depth chambers and the end plate, respectively. The total number and the position of the filaments can be changed. The each arc sub-chamber and the filter rods are electrically insulated. Ports for Langmuir probe measurement are provided so that the longitudinal scan and the transverse scans of the probes can be made.

The negative ion extraction electrode system consists of a plasma grid, an extraction grid, an electron suppression grid and a ground grid, as shown in Fig. 1 (b). Each grid is made of copper and has 400 holes of 9 mm in diameter in the area of 25×25 cm^2 (transparency of 40 %). The plasma grid and the extraction grid have water cooling channels inside the grids fabricated by the diffusion bonding technique. The extraction grid has another channels of the permanent magnet rows for the deflection of the extracted electrons. Large heat load of the extraction grid due to the bombardment of the deflected

electrons is one of the main problems in a high power negative ion source. In this ion source, as shown in Fig. 1 (c), the cooling channels are arranged perpendicularly against the permanent magnet rows so that the deflected electrons are incident on the vicinity of the cooling channels. As a result, effective cooling of the extraction grid is expected. Since the permanent magnet rows are packed in thin stainless steel cans and are inserted in the channels, the magnetic field strength can be changed by replacing them. The extracted beamlets are not focused (parallel beam). The extraction electrode system is electrically insulated against 120 kV with the insulator made of synthetic resin. The power supplies for the negative ion source are also shown in Fig. 1 (b).

The negative hydrogen ions were extracted at the extraction voltage, V_{ext}, of 2 to 5 kV and were accelerated at the acceleration voltage, V_{acc}, of 3 kV or more than 15 kV. The potential of the plasma grid was floating to that of the arc chamber. The electron suppression grid and the extraction grid were electrically connected in the experiments of V_{acc}=3 kV and the electron suppression voltage of 2 kV was applied in the experiments of V_{acc} of more than 15 kV. The beam pulse length was 0.3 sec.

The negative ion source is designed so flexibly that various kinds of configuration of the source can be tested and that the optimization of the negative ion production can be made. The experimental arrangement of the arc chamber in these experiments is shown in Fig. 2. In the double-magnetic filter configuration, a shallow arc chamber is preferable and one 14 cm-depth sub-chamber was used. The distance between the filaments and the chamber wall affects the discharge in the double-magnetic filter configuration and was set at about 40mm in these experiments. The cusp magnetic field strength on the wall surface is about 1kG and is decreased abruptly as the distance from

the wall is increased. At the position of the filaments, the field strength of the normal component to the wall is about 20G.

In these experiments, three kinds of the electron filter were examined; the total numbers of the rod were 3, 2, and zero (no filter field). The magnetic field strengths between the filter rods are 46, 26 and zero G, respectively. The accelerated negative ions are measured by a calorimeter array which is placed at a distance of about 1.6 m downstream of the plasma grid. The calorimeter array contains a series of seventeen calorimeters arranged in the X-direction in Fig.1(a) (horizontal). Although most of the extracted electrons are deflected by the magnetic field and impinge on the extraction grid, the residual electrons and the secondary electrons are accelerated. The accelerated electrons are removed by the magnetic field produced by the permanent magnet bars placed in front of the calorimeter array. A small amount of the accelerated electrons, however, were detected for the high energy beam. We measured the detected electron current for helium discharge and the leakage electron current was estimated to be several % of the measured current for the hydrogen discharge when the total acceleration energy was 35keV.

III. EXPERIMENTAL RESULTS

A. Discharge characteristics

In Fig.3 are shown the typical transverse profiles (in the X-direction in Fig. 1(a)) of the electron temperature, T_e, and the electron saturation current density, J_{es}, along the mid plane of the arc chamber (between the end plate and the electron filter). The profiles of the electron temperature and density are hollow, since the filaments are placed near the chamber wall and the fast electrons emitted from the filaments are trapped by the cusp field. The electron temperature in the central region is low and around 1 eV, and is not

much increased with an increase in the arc power. Under these conditions fast electrons producing vibrationally excited hydrogen molecules (H_2^*) are localized near the wall. On the contrary, in the central region there exist only the thermal electrons with relatively low temperature. The negative hydrogen ions are produced there by collisions between the H_2^* and the thermal electrons, and diffuse to the extraction region. The H_2^* molecules also reach the extraction region unaffected by the electron filter field, and the negative hydrogen ions are also produced there. In this configuration the electron filter field is utilized for control of the electron density in the extraction region rather than that of the electron temperature. Moreover, it is expected that the production of the H_2^* by collisions of H_2^+ and H_3^+ ions to the chamber wall should be enhanced because the plasma density near the wall is high in this configuration[12].

Figures 4 (a) and (b) show the longitudinal profiles (in the Z-direction) of the electron saturation current densities and the electron temperatures for the three different electron filter field strengths. The decrement of the electron density from the production region to the extraction region through the electron filter is much dependent on the filter field strength. The electron density in front of the plasma grid is lower at the higher filter field strength. On the other hand, the electron temperature seems to be not much affected by the electron filter strength. In the case of the no rod, the electron temperature is a little higher than those in the cases of the 2 and 3 rods.

B. H^- ion extraction characteristics

The H^- ion extraction characteristics for the three different electron filter field strengths are shown in Fig. 5. The H^- ion current densities measured by the central calorimeter and the extraction currents as a function

of the arc power are shown in Figs. 5 (a) and (b), respectively. The electron saturation current density in front of the plasma grid for the 2 rods is also shown in Fig. 5 (b). The extraction voltage was 2 kV and the acceleration voltage 3 kV (the total beam energy was 5 keV). For these low energy beams, the H^- ion beam profile was not much changed by the arc power. Although the H^- ion current is a little larger for the lower filter strength at the lower arc power, the H^- ion currents are nearly equal for the three filter strengths. On the other hand, the extraction current is larger for the lower filter strength. The extraction currents are increased with an increase in the arc power, corresponding to an increase in the electron density in front of the plasma grid. Therefore, it is found that the electron filter controls the extracted electron current independently of the H^- ion current.

The dependence of the H^- ion current densities and the extraction currents on the gas pressure for the 3 rods are shown in Figs. 6 (a) and (b), respectively. The beam energy was 5 keV. The optimum gas pressure for the H^- ion yield tends to be higher at the higher arc power. The extraction current is decreased as the gas pressure is increased. This corresponds to the gas pressure dependence of the electron density in front of the plasma grid.

In these experiments, we changed the arc power by changing the arc voltage and current simultaneously, and the arc voltage ranged from 45 to 70 V. It is important to know the dependence on the arc voltage of the H^- ion production. The H^- ion current densities and the extraction currents in the 3 rods case are shown in Figs. 7 (a) and (b), respectively, as a function of the arc power for the four fixed arc voltages. It is found that the H^- ion current and the extraction current are almost independent of the arc voltage, although it seems that at the lower arc voltage the H^- ion current is higher and the

extraction current is lower. Since the production efficiency of the H_2^* by the electron impact is dependent on the fast electron energy, the wall collision of the H_2^+ and the H_3^+ may contribute to the H_2^* production to some extent in the double-magnetic filter configuration.

Figure 8 (a) shows the dependence on the extraction voltage of the total H^- ion current calculated from the local H^- ion current densities measured by the calorimeter array. As the arc power is increased, the optimum extraction voltage becomes higher. The extraction current is almost independent of the extraction voltage, as shown in Fig. 8 (b). The H^- ion current dependence on the extraction voltage is related with the extraction optics. Generally, the optimum extraction voltage is determined so that the space-charge-limited current should be equal to the H^- ion saturation current in the extraction region. Since the H^- ion density in the extraction region is increased with an increase in the arc power, the corresponding optimum extraction voltage is also increased. On the other hand, the electron saturation current in the extraction region is so low compared with the space-charge-limited current of the electron that the extraction current is not influenced by the extraction voltage.

The beam profile was changed by the extraction voltage when the acceleration voltage was high. Figure 9 shows the H^- ion beam profiles for the various extraction voltages at the fixed arc power of 49 kW and at the acceleration voltage of 30 kV. The beam profile becomes more peaked as the extraction voltage is increased. So far, we have obtained a 1.4 A of the H^- ion current with the energy of 34 keV at the arc power of 59 kW.

IV. DISCUSSION

In the double-magnetic filter configuration, the main arc discharge plasma containing many fast electrons is localized near the chamber wall by the cusp field. Thus, the region near the wall is a driver region where the vibrationally excited molecules, H_2^*, are generated. On the other hand, the central region where the plasma has electrons with low temperature is a production region of the negative ions. This configuration has the similar operational principle to the hybrid multicusp ion source studied at the Ecole Polytechnique[13] and the tent filter ion source at the Culham Laboratory[14]. In this ion source the magnetic filter in front of the plasma grid acts as the electron filter. Thus, the electron density in the extraction region can be controlled by the electron filter field strength independently of the H^- ion production. The rod magnetic filter is not necessarily proper for the electron filter, because the H^- ions can be destroyed on the rod surfaces. We have to devise the better method for the electron filter to optimize the double-magnetic filter configuration. The H^- ion temperature has been reported to be around 0.1eV[15]. Then, the dominant process of the H^- ion destruction is the mutual neutralization by collisions with the positive ions (H^+,H_2^+ and H_3^+) in the production and the extraction regions. Under this experimental condition, the mean free path of the mutual neutralization is estimated to be more than 10cm. Therefore, the H^- ions generated in the central region can reach the plasma grid. The double-magnetic filter configuration is related with the position of the filaments. The localized discharge with the hollow plasma profiles was not observed when the distance between the filaments and the wall was more than 80 mm. In this case the normal discharge with flat or peak profiles of the electron density and temperature was observed, and the negative ions were produced in the single-magnetic filter configuration, where

the central region is the driver region. The comparison between the double- and the single-magnetic filter configurations is described in detail in ref.11. The gas pressure also affects the localized discharge. As the gas pressure was lower, the electron temperature in the central region became higher and the hollowness of the profiles of the electron temperature and density also became smaller. The electron density in the production region, i.e., the central region, is high of more than 2×10^{12} cm^{-3}. A preliminary result from the measurement of the H^- ion density by the photo-detachment technique shows that the H^- ion density in the central region is almost equal to the electron density. The measured total H^- ion current is too small compared with the H^- ion density, even if considering the stripping loss. This suggests that the extraction mechanism of the H^- ions should be investigated in more detail.

ACKNOWLEDGMENTS

The authors would like to thank Messrs. R. Akiyama, T. Kawamoto, A. Karita and K. Mineo for their assistances of the experiments.

REFERENCES

1) A.Iiyoshi, Proc. of the 13th Symp. on Fusion Engineering, Knoxville (1989), p. 1007.

2) O.Motojima, K.Akaishi, M.Asao, K.Fujii, J.Fujita, et al., Proc. the 13th Inter. Conf. on Plasma Physics and Controlled Nuclear Fusion Research, Washington. DC (1990), paper No. IAEA-CN-53/G-1-5.

3) T.Mutoh, Y.Takeiri, T.Obiki, F.Sato, A.Fukuyama, et al., Proc. of the 15th Symp. on Fusion Technology, Utrecht (1988), p. 552.

4) Y.Takeiri, O.Kaneko, F.Sano, A.Ando, Y.Oka, et al., Proc. of the 1st Int. Toki Conf. on Plasma Physics and Controlled Nuclear Fusion, Toki, Japan (1989), p.272.

5) T.Inoue, M.Araki, M.Hanada, T.Kurashima, S.Matsuda, et al., Nucl. Instr. Meth. **B37/38**, 111 (1989).

6) A.J.T.Holmes, L.M.Lea, A.F.Newman, and M.P.S.Nightingale, Rev. Sci. Instrum. **58**, 223 (1987).

7) K.N.Leung, K.W.Ehlers, C.A.Hauck, W.B.Kunkel, and A.F.Lietzke, Rev. Sci.Instrum. **59**, 453 (1988).

8) Y.Ohara, M.Akiba, M.Araki, M.Hanada, T.Inoue, et.al., Proc. of the 13th Symp. on Fusion Engineering, Knoxville (1989), p.284.

9) Y.Okumura, M.Hanada, T.Inoue, H.Kojima, Y.Matsuoka, et al., Proc. of the 16th Symp. on Fusion Technology, London (1990), (to be published).

10) Y. Takeiri, A. Ando, O. Kaneko, Y. Oka, R.Akiyama, et al., Proc. of the 16th Symp. on Fusion Technology, London (1990), (to be published).

11) A.Ando, Y.Takeiri, O.Kaneko, Y.Oka, M.Wada, and T.Kuroda (to be submitted).

12) J.R.Hiskes and A.M.Karo, J. Appl. Phys. **67**, 6621 (1990).

13) M.Bacal, A.M.Bruneteau, and M.Nachman, J. Appl. Phys. **55**, 15 (1984).

14) L.M.Lea, A.J.T.Holmes, M.F.Thornton, and G.O.R.Naylor, Rev. Sci. Instrum. **61**, 409 (1990).

15) P.Devynck, J.Auvray, M.Bacal, P.Berlemout, J.Bruneteau, R.Leroy, and R.A.Stern, Rev. Sci. Instrum. **60**,2873 (1989).

FIGURE CAPTION

Fig. 1

(a) Schematic diagram of the ion source, (b) negative ion extraction system, and (c) structure of the extraction grid.

Fig. 2

Experimental arrangement of the arc chamber for the double-magnetic filter configuration.

Fig. 3

Transverse profiles (in the X-direction) of the electron temperature and the electron saturation current density in the central region of the arc chamber. The gas pressure was 14 mTorr and the arc power 45 kW.

Fig. 4

Longitudinal profiles (in the Z-direction) of (a) electron saturation current densities and (b) electron temperatures for the three different electron filter field strengths. The gas pressure was 14 mTorr and the arc power 45 kW.

Fig. 5

(a) H^- ion current densities measured by the central calorimeter and (b) extraction currents as a function of the arc power for the three different electron filter fields. The electron saturation current density in front of the plasma grid for the 2 rods is also shown in (b). The gas pressure was 14 mTorr.

Fig. 6

Dependence of (a) H^- ion current densities and (b) extraction currents on the gas pressure for the 3 rods. Parameter is the arc power. The beam energy was 5 keV.

Fig. 7

(a) H^- ion current densities and (b) extraction currents for the 3 rods as a function of the arc power for the four fixed arc voltages; 62 V, 72 V, 82 V and 91 V. The extraction voltage was 3 kV and the acceleration voltage 17 kV. The gas pressure was 11 mTorr.

Fig. 8

Dependence of (a) total H^- ion currents and (b) extraction currents on the extraction voltage for the 3 rods. Parameter is the arc power. The acceleration voltage was 30 kV and the gas pressure 11 mTorr.

Fig. 9

H^- beam profiles for the various extraction voltages. The acceleration voltage was 30 kV, the arc power 49 kW and the gas pressure 11 mTorr.

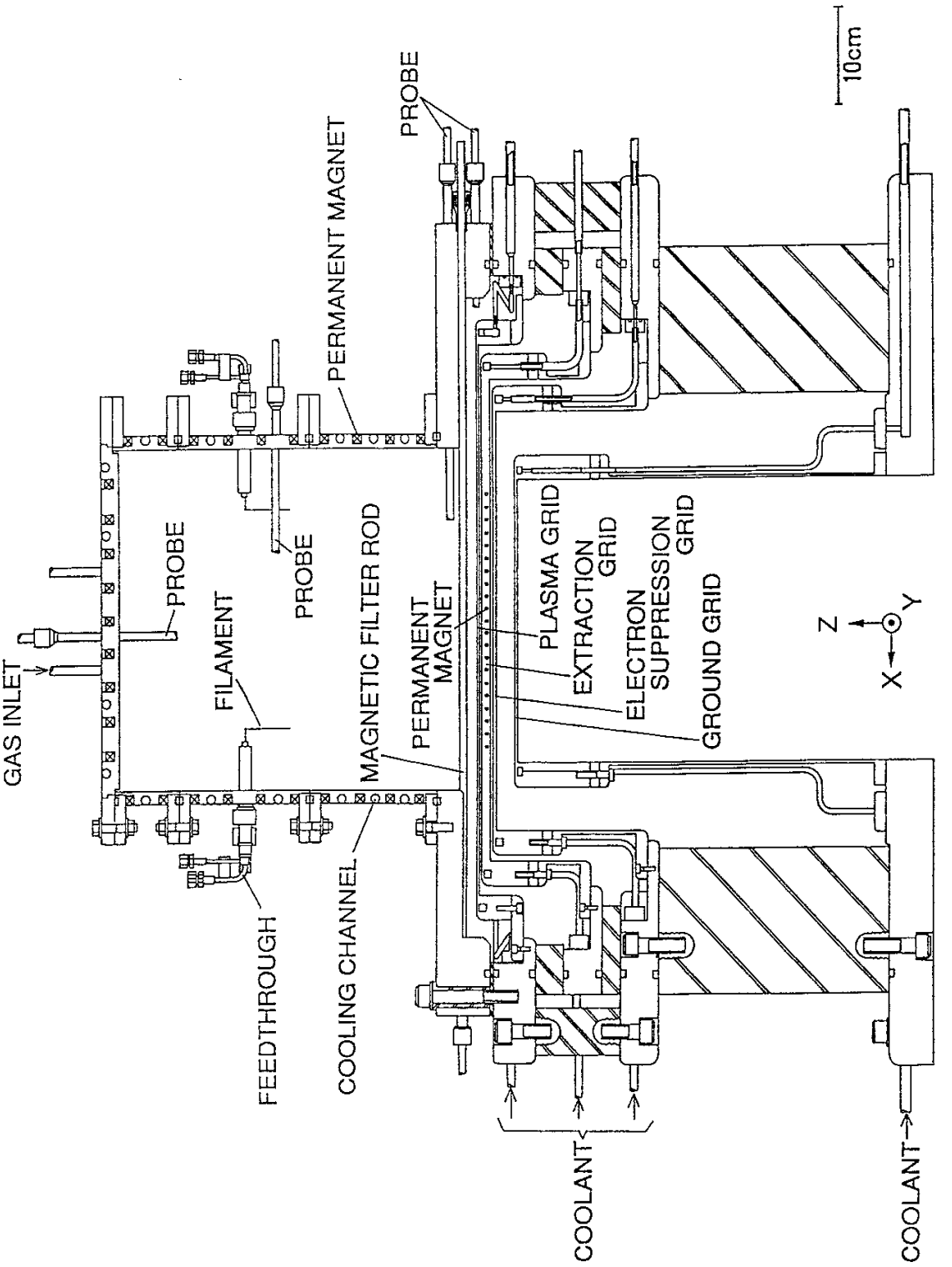
GAS INLET
PROBE
FILAMENT
PROBE
MAGNETIC FILTER ROD
PERMANENT MAGNET
PERMANENT MAGNET
PROBE
PLASMA GRID
EXTRACTION GRID
ELECTRON SUPPRESSION GRID
GROUND GRID
FEEDTHROUGH
COOLING CHANNEL
COOLANT
COOLANT
10cm
Z
Y
X

Fig. 1 (a)

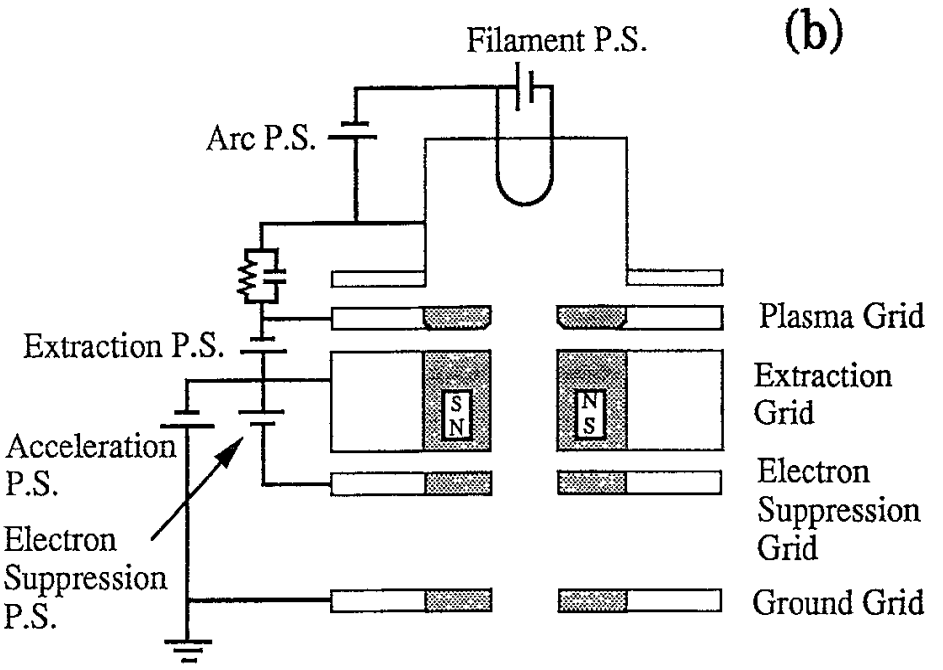
(b)
Filament P.S.
Arc P.S.
Extraction P.S.
Acceleration P.S.
Electron Suppression P.S.
Plasma Grid
Extraction Grid
Electron Suppression Grid
Ground Grid
S
N
N
S

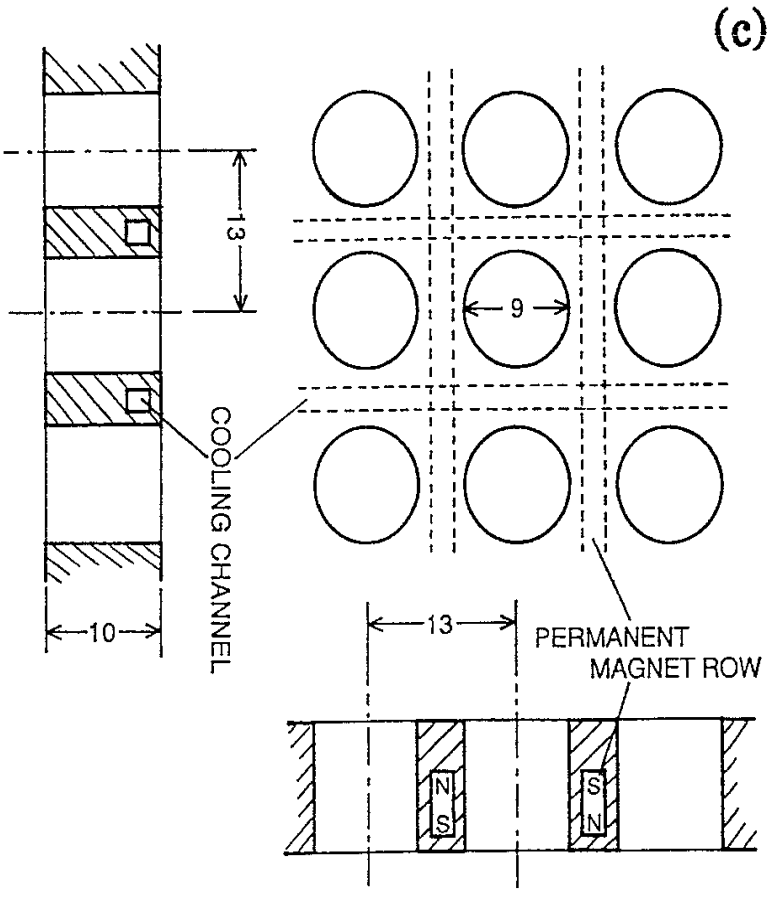
(c)
13
9
10
COOLING CHANNEL
13
PERMANENT MAGNET ROW
N
S
S
N

Fig. 1

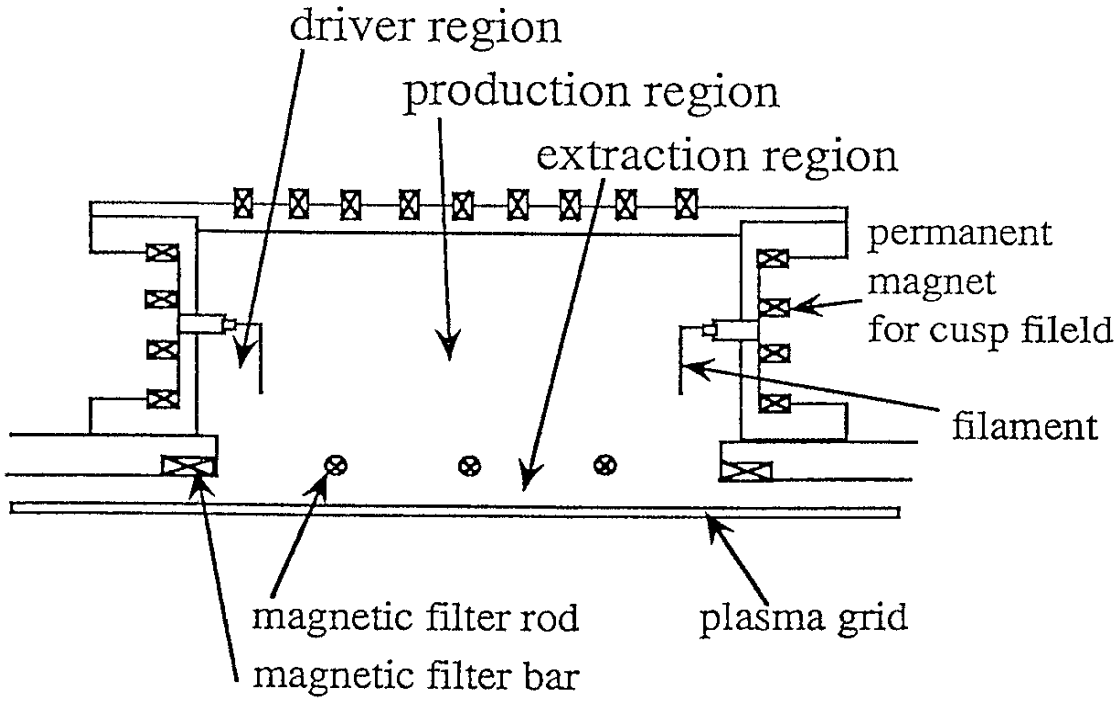
driver region
production region
extraction region
permanent
magnet
for cusp fileld
filament
magnetic filter rod
magnetic filter bar
plasma grid

Fig. 2

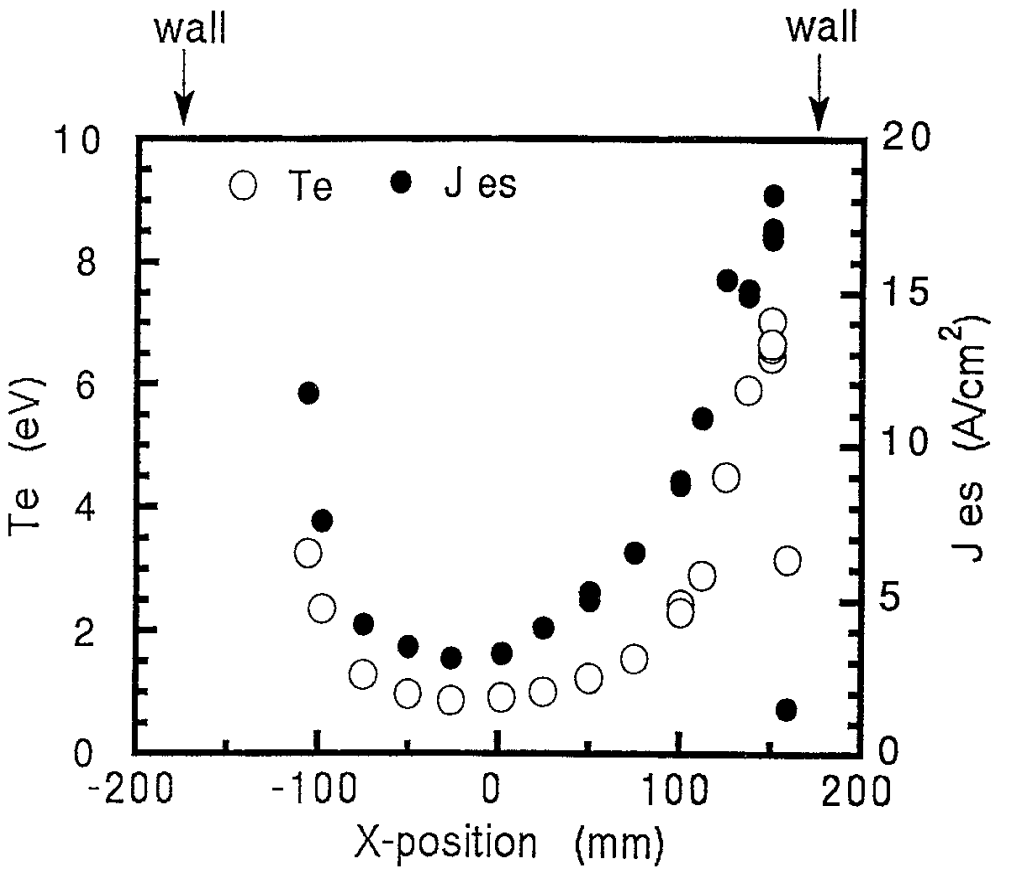
wall
wall
Te
J es
10
8
6
4
2
0
20
15
10
5
0
-200
-100
0
100
200
Te (eV)
J es (A/cm^2)
X-position (mm)

Fig. 3

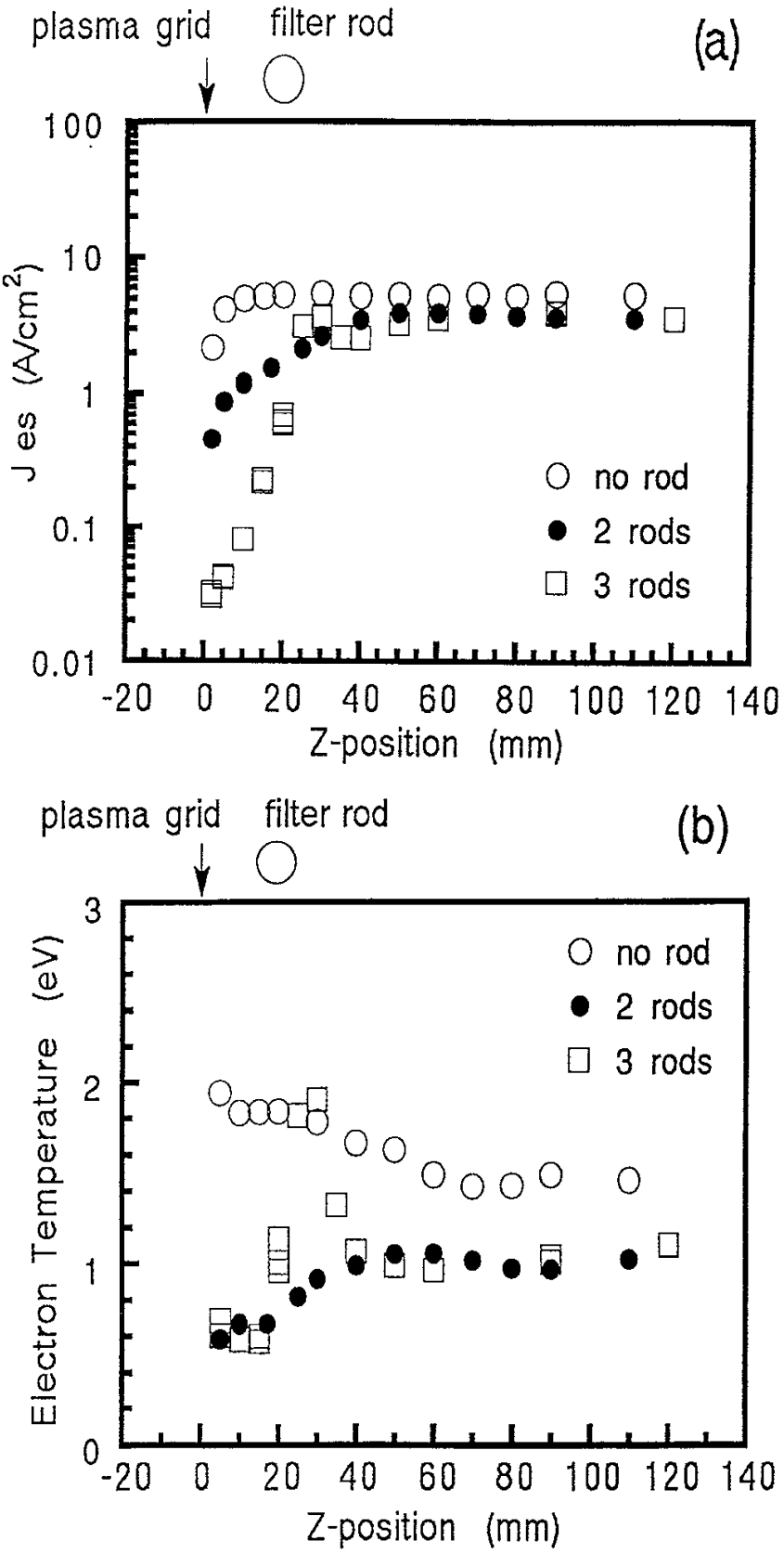
plasma grid
filter rod
(a)
100
10
1
0.1
0.01
J es (A/cm^2)
no rod
2 rods
3 rods
-20
0
20
40
60
80
100
120
140
Z-position (mm)
plasma grid
filter rod
(b)
3
2
1
0
Electron Temperature (eV)
no rod
2 rods
3 rods
-20
0
20
40
60
80
100
120
140
Z-position (mm)

Fig. 4

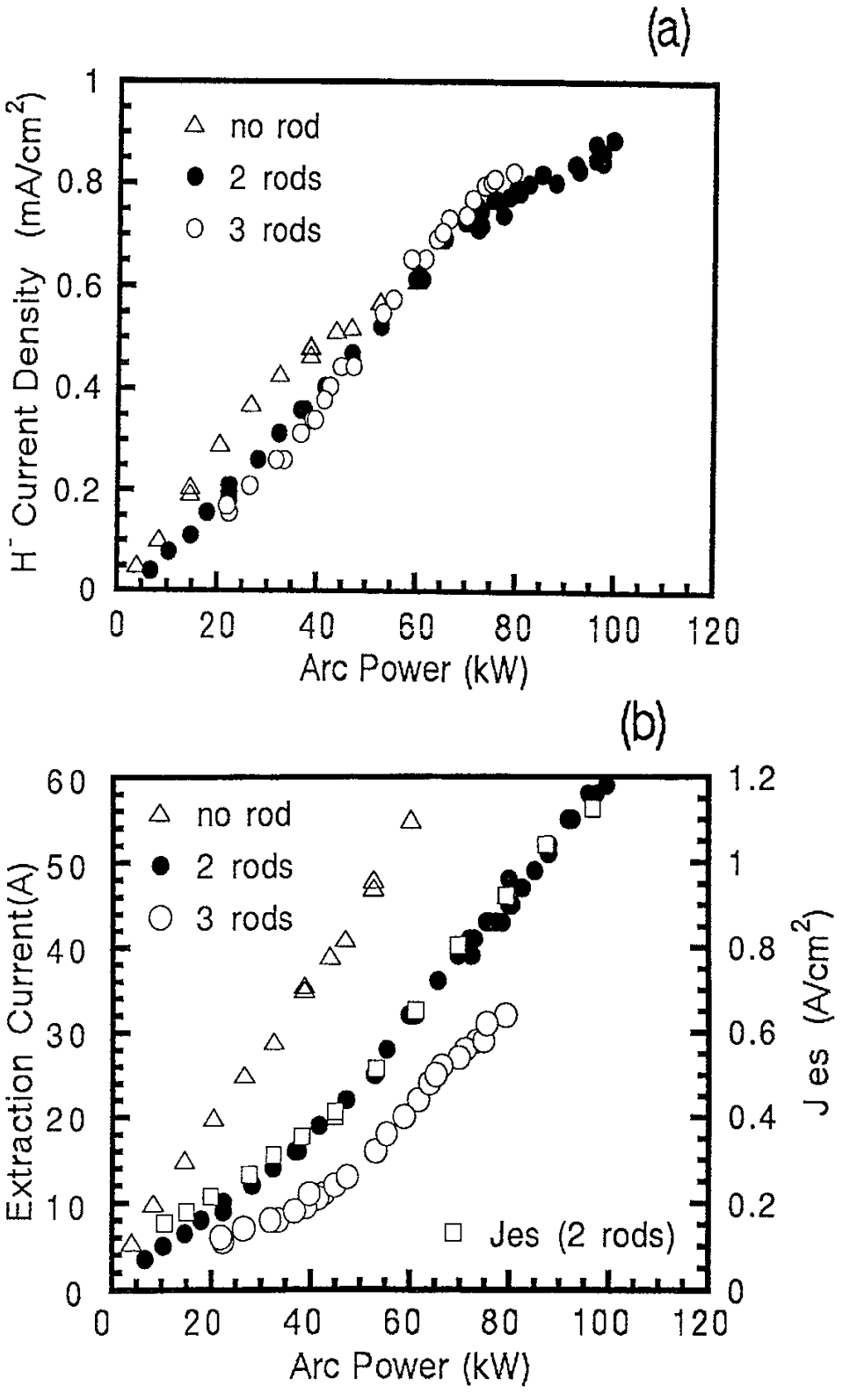
(a)
no rod
2 rods
3 rods
H⁻ Current Density (mA/cm²)
Arc Power (kW)
(b)
no rod
2 rods
3 rods
Jes (2 rods)
Extraction Current(A)
J es (A/cm²)
Arc Power (kW)

Fig. 5

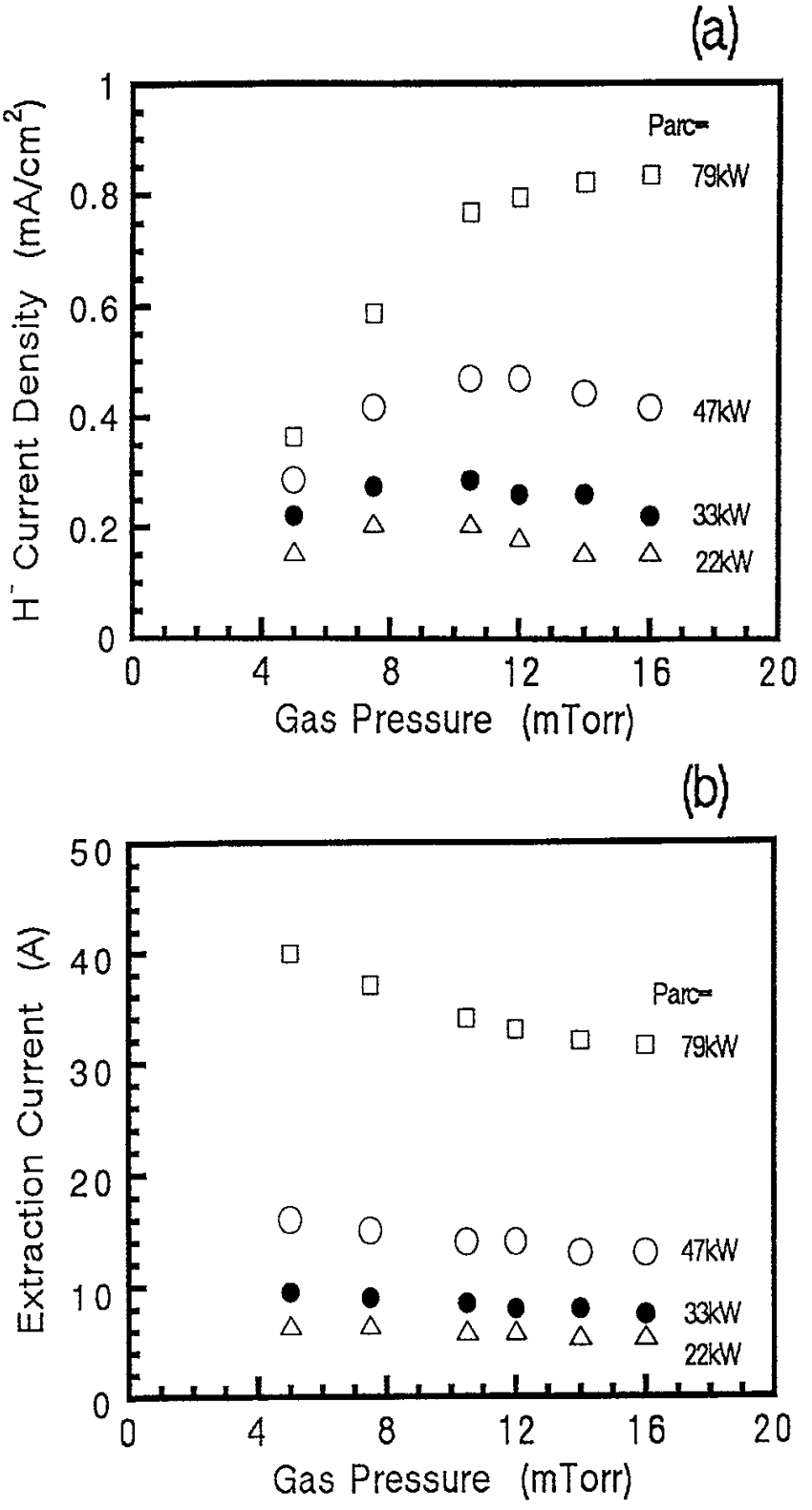
(a)
H⁻ Current Density (mA/cm²)
1
0.8
0.6
0.4
0.2
0
Parc=
79kW
47kW
33kW
22kW
0
4
8
12
16
20
Gas Pressure (mTorr)
(b)
Extraction Current (A)
50
40
30
20
10
0
Parc=
79kW
47kW
33kW
22kW
0
4
8
12
16
20
Gas Pressure (mTorr)

Fig. 6

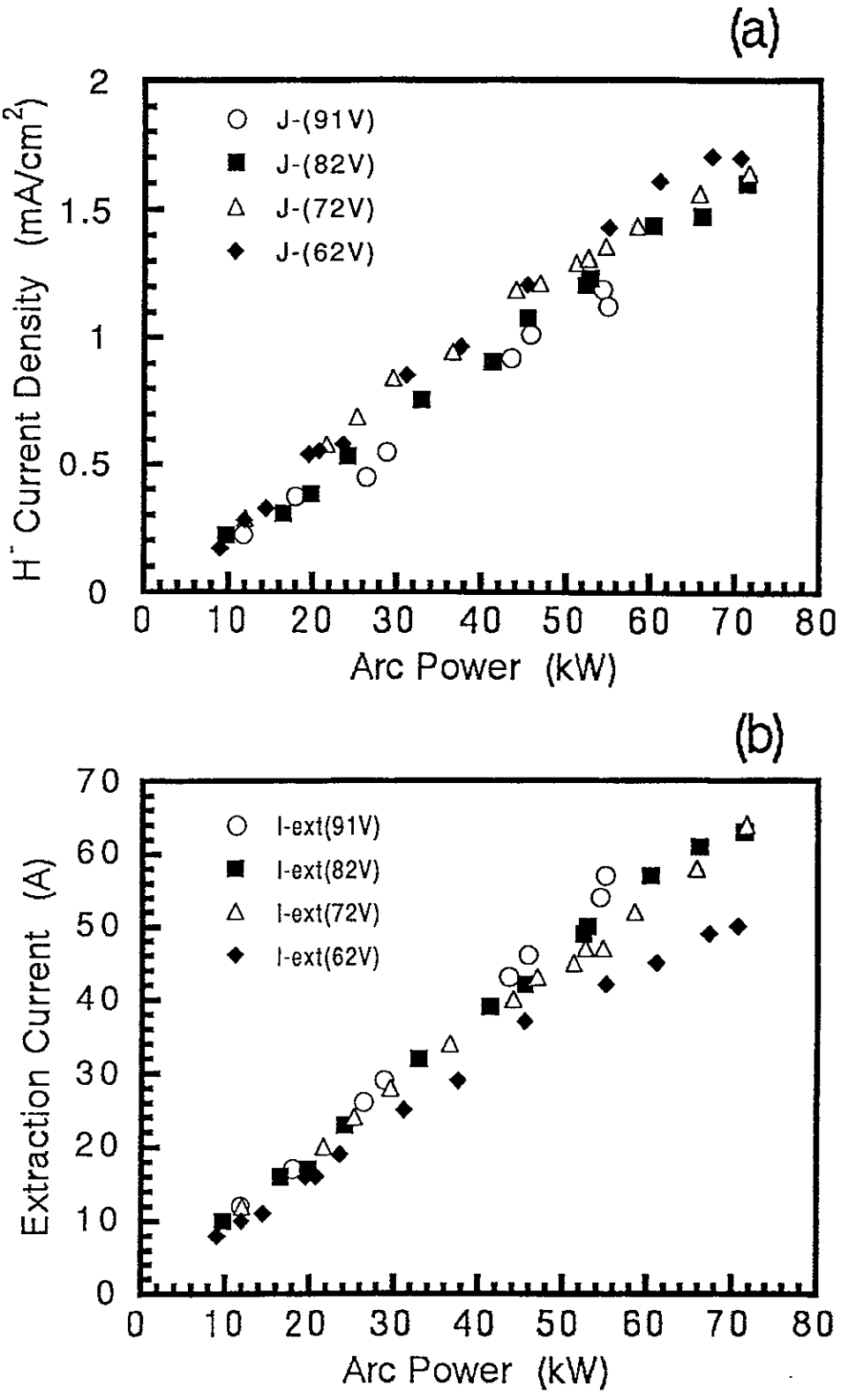
(a)
H⁻ Current Density (mA/cm²)
J-(91V)
J-(82V)
J-(72V)
J-(62V)
Arc Power (kW)
(b)
Extraction Current (A)
I-ext(91V)
I-ext(82V)
I-ext(72V)
I-ext(62V)
Arc Power (kW)

Fig. 7

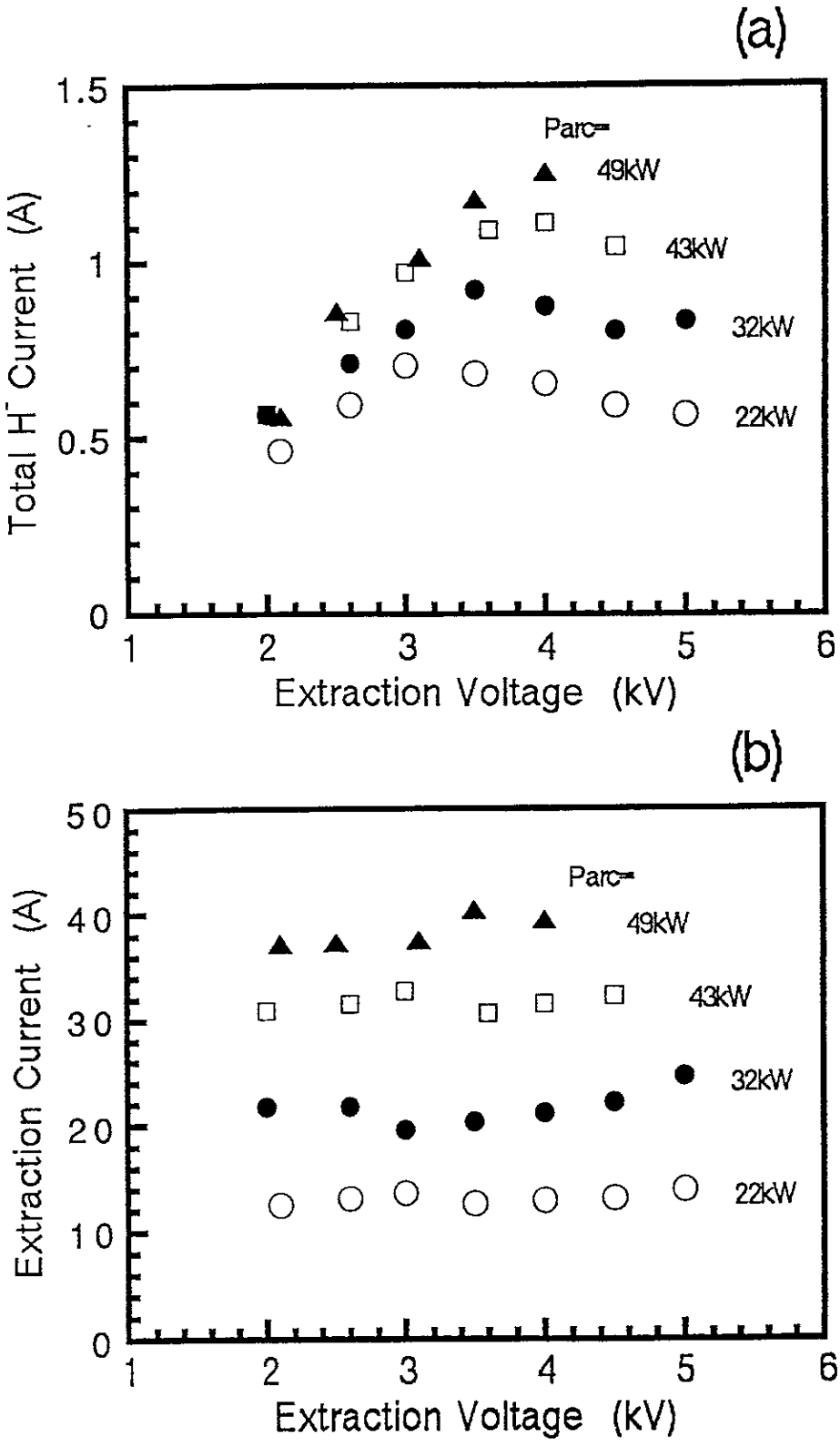
(a)
Total H⁻ Current (A)
1.5
1
0.5
0
Parc=
49kW
43kW
32kW
22kW
1
2
3
4
5
6
Extraction Voltage (kV)
(b)
Extraction Current (A)
50
40
30
20
10
0
Parc=
49kW
43kW
32kW
22kW
1
2
3
4
5
6
Extraction Voltage (kV)

Fig. 8

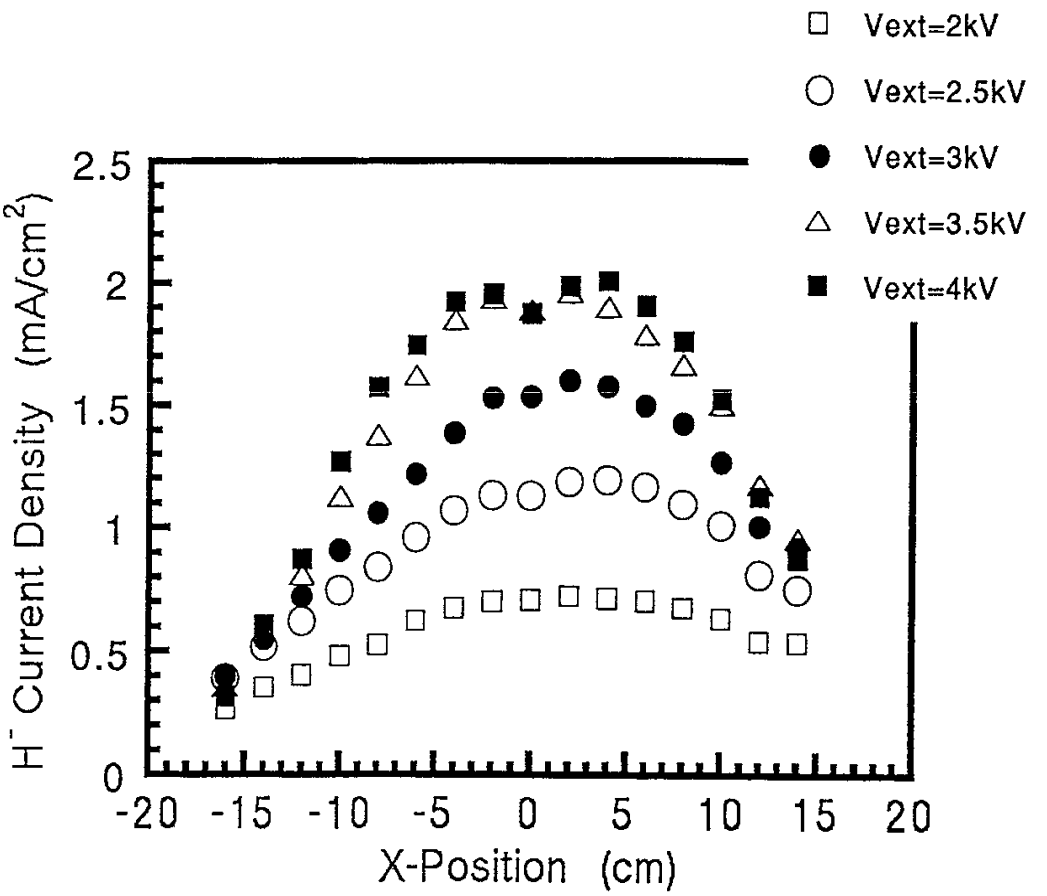
Vext=2kV
Vext=2.5kV
Vext=3kV
Vext=3.5kV
Vext=4kV
H- Current Density (mA/cm2)
2.5
2
1.5
1
0.5
0
-20
-15
-10
-5
0
5
10
15
20
X-Position (cm)

Fig. 9

Recent Issues of NIFS Series

NIFS-100 H. Hojo, T. Ogawa and M. Kono, *Fluid Description of Ponderomotive Force Compatible with the Kinetic One in a Warm Plasma* ; July 1991

NIFS-101 H. Momota, A. Ishida, Y. Kohzaki, G. H. Miley, S. Ohi, M. Ohnishi K. Yoshikawa, K. Sato, L. C. Steinhauer, Y. Tomita and M. Tuszewski *Conceptual Design of D-^{3}He FRC Reactor "ARTEMIS"* ; July 1991

NIFS-102 N. Nakajima and M. Okamoto, *Rotations of Bulk Ions and Impurities in Non-Axisymmetric Toroidal Systems* ; July 1991

NIFS-103 A. J. Lichtenberg, K. Itoh, S. - I. Itoh and A. Fukuyama, *The Role of Stochasticity in Sawtooth Oscillation* ; Aug. 1991

NIFS-104 K. Yamazaki and T. Amano, *Plasma Transport Simulation Modeling for Helical Confinement Systems;* Aug. 1991

NIFS-105 T. Sato, T. Hayashi, K. Watanabe, R. Horiuchi, M. Tanaka, N. Sawairi and K. Kusano, *Role of Compressibility on Driven Magnetic Reconnection ;* Aug. 1991

NIFS-106 Qian Wen - Jia, Duan Yun - Bo, Wang Rong - Long and H. Narumi, *Electron Impact Excitation of Positive Ions - Partial Wave Approach in Coulomb - Eikonal Approximation* ; Sep. 1991

NIFS-107 S. Murakami and T. Sato, *Macroscale Particle Simulation of Externally Driven Magnetic Reconnection;* Sep. 1991

NIFS-108 Y. Ogawa, T. Amano, N. Nakajima, Y. Ohyabu, K. Yamazaki, S. P. Hirshman, W. I. van Rij and K. C. Shaing, *Neoclassical Transport Analysis in the Banana Regime on Large Helical Device (LHD) with the DKES Code;* Sep. 1991

NIFS-109 Y. Kondoh, *Thought Analysis on Relaxation and General Principle to Find Relaxed State;* Sep. 1991

NIFS-110 H. Yamada, K. Ida, H. Iguchi, K. Hanatani, S. Morita, O. Kaneko, H. C. Howe, S. P. Hirshman, D. K. Lee, H. Arimoto, M. Hosokawa, H. Idei, S. Kubo, K. Matsuoka, K. Nishimura, S. Okamura, Y. Takeiri, Y. Takita and C. Takahashi, *Shafranov Shift in Low-Aspect-Ratio Heliotron / Torsatron CHS* ; Sep 1991

NIFS-111 R. Horiuchi, M. Uchida and T. Sato, *Simulation Study of Stepwise Relaxation in a Spheromak Plasma ;* Oct. 1991

NIFS-112 M. Sasao, Y. Okabe, A. Fujisawa, H. Iguchi, J. Fujita, H. Yamaoka and M. Wada, *Development of Negative Heavy Ion Sources for Plasma Potential Measurement* ; Oct. 1991

NIFS-113 S. Kawata and H. Nakashima, *Tritium Content of a DT Pellet in Inertial Confinement Fusion* ; Oct. 1991

NIFS-114 M. Okamoto, N. Nakajima and H. Sugama, *Plasma Parameter Estimations for the Large Helical Device Based on the Gyro-Reduced Bohm Scaling* ; Oct. 1991

NIFS-115 Y. Okabe, *Study of Au^- Production in a Plasma-Sputter Type Negative Ion Source* ; Oct. 1991

NIFS-116 M. Sakamoto, K. N. Sato, Y. Ogawa, K. Kawahata, S. Hirokura, S. Okajima, K. Adati, Y. Hamada, S. Hidekuma, K. Ida, Y. Kawasumi, M. Kojima, K. Masai, S. Morita, H. Takahashi, Y. Taniguchi, K. Toi and T. Tsuzuki, *Fast Cooling Phenomena with Ice Pellet Injection in the JIPP T-IIU Tokamak;* Oct. 1991

NIFS-117 K. Itoh, H. Sanuki and S. -I. Itoh, *Fast Ion Loss and Radial Electric Field in Wendelstein VII-Λ Stellarator;* Oct. 1991

NIFS-118 Y. Kondoh and Y. Hosaka, *Kernel Optimum Nearly-analytical Discretization (KOND) Method Applied to Parabolic Equations <<KOND-P Scheme>>;* Nov. 1991

NIFS-119 T. Yabe and T. Ishikawa, *Two- and Three-Dimensional Simulation Code for Radiation-Hydrodynamics in ICF*; Nov. 1991

NIFS-120 S. Kawata, M. Shiromoto and T. Teramoto, *Density-Carrying Particle Method for Fluid* ; Nov. 1991

NIFS-121 T. Ishikawa, P. Y. Wang, K. Wakui and T. Yabe, *A Method for the High-speed Generation of Random Numbers with Arbitrary Distributions;* Nov. 1991

NIFS-122 K. Yamazaki, H. Kaneko, Y. Taniguchi, O. Motojima and LHD Design *Group, Status of LHD Control System Design ; Dec. 1991*

NIFS-123 Y. Kondoh, *Relaxed State of Energy in Incompressible Fluid and Incompressible MHD Fluid* ; Dec. 1991

NIFS-124 K. Ida, S. Hidekuma, M. Kojima, Y. Miura, S. Tsuji, K. Hoshino, M. Mori, N. Suzuki, T. Yamauchi and JFT-2M Group, *Edge Poloidal Rotation Profiles of H-Mode Plasmas in the JFT-2M Tokamak ;*

Dec. 1991

NIFS-125 H. Sugama and M. Wakatani, *Statistical Analysis of Anomalous Transport in Resistive Interchange Turbulence* ;Dec. 1991

NIFS-126 K. Narihara, *A Steady State Tokamak Operation by Use of Magnetic Monopoles* ; Dec. 1991

NIFS-127 K. Itoh, S. -I. Itoh and A. Fukuyama, *Energy Transport in the Steady State Plasma Sustained by DC Helicity Current Drive* ;Jan. 1992

NIFS-128 Y. Hamada, Y. Kawasumi, K. Masai, H. Iguchi, A. Fujisawa, JIPP T-IIU Group and Y. Abe, *New Hight Voltage Parallel Plate Analyzer* ; Jan. 1992

NIFS-129 K. Ida and T. Kato, *Line-Emission Cross Sections for the Charge-exchange Reaction between Fully Stripped Carbon and Atomic Hydrogen in Tokamak Plasma*; Jan. 1992

NIFS-130 T. Hayashi, A. Takei and T. Sato, *Magnetic Surface Breaking in 3D MHD Equilibria of l=2 Heliotron* ; Jan. 1992

NIFS-131 K. Itoh, K. Ichiguchi and S. -I. Itoh, *Beta Limit of Resistive Plasma in Torsatron/Heliotron* ; Feb. 1992

NIFS-132 K. Sato and F. Miyawaki, *Formation of Presheath and Current-Free Double Layer in a Two-Electron-Temperature Plasma* ; Feb. 1992

NIFS-133 T. Maruyama and S. Kawata, *Superposed-Laser Electron Acceleration* Feb. 1992

NIFS-134 Y. Miura, F. Okano, N. Suzuki, M. Mori, K. Hoshino, H. Maeda, T. Takizuka, JFT-2M Group, S.-I. Itoh and K. Itoh, *Rapid Change of Hydrogen Neutral Energy Distribution at L/H-Transition in JFT-2M H-mode ;* Feb. 1992

NIFS-135 H. Ji, H. Toyama, A. Fujisawa, S. Shinohara and K. Miyamoto *Fluctuation and Edge Current Sustainment in a Reversed-Field-Pinch;* Feb. 1992

NIFS-136 K. Sato and F. Miyawaki, *Heat Flow of a Two-Electron-Temperature Plasma through the Sheath in the Presence of Electron Emission;* Mar. 1992

NIFS-137 T. Hayashi, U. Schwenn and E. Strumberger, *Field Line Diversion Properties of Finite ß Helias Equilibria;* Mar. 1992

NIFS-138 T. Yamagishi, *Kinetic Approach to Long Wave Length Modes in*

Rotating Plasmas; Mar. 1992

NIFS-139 K. Watanabe, N. Nakajima, M. Okamoto, Y. Nakamura and M. Wakatani, *Three-dimensional MHD Equilibrium in the Presence of Bootstrap Current for Large Helical Device (LHD)*; Mar. 1992

NIFS-140 K. Itoh, S. -I. Itoh and A. Fukuyama, *Theory of Anomalous Transport in Toroidal Helical Plasmas;* Mar. 1992

NIFS-141 Y. Kondoh, *Internal Structures of Self-Organized Relaxed States and Self-Similar Decay Phase;* Mar. 1992

NIFS-142 U. Furukane, K. Sato, K. Takiyama and T. Oda, *Recombining Processes in a Cooling Plasma by Mixing of Initially Heated Gas*; Mar. 1992

NIFS-143 Y. Hamada, K. Masai, Y. Kawasumi, H. Iguchi, A. Fijisawa and JIPP T-IIU Group, *New Method of Error Elimination in Potential Profile Measurement of Tokamak Plasmas by High Voltage Heavy Ion Beam Probes;* Apr. 1992

NIFS-144 N. Ohyabu, N. Noda, Hantao Ji, H. Akao, K. Akaishi, T. Ono, H. Kaneko, T: Kawamura, Y. Kubota, S. Morimoto. A. Sagara, T. Watanabe, K. Yamazaki and O. Motojima, *Helical Divertor in the Large Helical Device;* May 1992

NIFS-145 K. Ohkubo and K. Matsumoto, *Coupling to the Lower Hybrid Waves with the Multijunction Grill*; May 1992

NIFS-146 K. Itoh, S. -I.Itoh, A. Fukuyama, S. Tsuji and Allan J. Lichtenberg, *A Model of Major Disruption in Tokamaks*; May 1992

NIFS-147 S. Sasaki, S. Takamura, M. Ueda, H. Iguchi, J. Fujita and K. Kadota, *Edge Plasma Density Reconstruction for Fast Monoenergetic Lithium Beam Probing*; May 1992

NIFS-148 N.Nakajima, C. Z. Cheng and M. Okamoto, *High-n Helicity-induced Shear Alfvén Eigenmodes*; May 1992

NIFS-149 A. Ando, Y. Takeiri, O. Kaneko, Y. Oka, M. Wada, and T. Kuroda, *Production of Negative Hydrogen Ions in a Large Multicusp Ion Source with Double-Magnetic Filter Configuration*; May 1992

NIFS-150 N. Nakajima and M. Okamoto, *Effects of Fast Ions and an External Inductive Electric Field on the Neoclassical Parallel Flow, Current, and Rotation in General Toroidal Systems*; May 1992